


ARTICLE

<https://doi.org/10.1038/s41467-020-14346-5>

OPEN

Ice I_c without stacking disorder by evacuating hydrogen from hydrogen hydrate

Kazuki Komatsu ^{1*}, Shinichi Machida², Fumiya Noritake^{3,4}, Takanori Hattori⁵, Asami Sano-Furukawa⁵, Ryo Yamane¹, Keishiro Yamashita¹ & Hiroyuki Kagi¹

Water freezes below 0 °C at ambient pressure ordinarily to ice I_h , with hexagonal stacking sequence. Under certain conditions, ice with a cubic stacking sequence can also be formed, but ideal ice I_c without stacking-disorder has never been formed until recently. Here we demonstrate a route to obtain ice I_c without stacking-disorder by degassing hydrogen from the high-pressure form of hydrogen hydrate, C_2 , which has a host framework isostructural with ice I_c . The stacking-disorder free ice I_c is formed from C_2 via an intermediate amorphous or nano-crystalline form under decompression, unlike the direct transformations occurring in ice XVI from neon hydrate, or ice XVII from hydrogen hydrate. The obtained ice I_c shows remarkable thermal stability, until the phase transition to ice I_h at 250 K, originating from the lack of dislocations. This discovery of ideal ice I_c will promote understanding of the role of stacking-disorder on the physical properties of ice as a counter end-member of ice I_h .

¹Geochemical Research Center, Graduate School of Science, The University of Tokyo, 7-3-1 Hongo, Bunkyo-ku, Tokyo 113-0033, Japan. ²Neutron Science and Technology Center, CROSS, 162-1 Shirakata, Tokai, Naka, Ibaraki 319-1106, Japan. ³Graduate Faculty of Interdisciplinary Research, University of Yamanashi, 4-3-11 Takeda, Kofu, Yamanashi 400-8511, Japan. ⁴Computational Engineering Applications Unit, RIKEN, 2-1 Hirosawa, Wako, Saitama 351-0198, Japan. ⁵J-PARC Center, Japan Atomic Energy Agency, 2-4 Shirakata, Tokai, Naka, Ibaraki 319-1195, Japan. *email: kom@eqchem.s.u-tokyo.ac.jp

Water freezes below 0 °C at ambient pressure, ordinarily to ice I_h with a hexagonal stacking sequence. However, it is also known to produce “ice I_c ” nominally with a cubic stacking sequence under certain conditions¹, and its existence in Earth’s atmosphere^{2–4}, or in comets^{5,6} is debated. “Ice I_c ”, or called as cubic ice, was first identified in 1943 by König⁷, who used electron microscopy to study the condensation of ice from water vapor to a cold substrate. Subsequently, many different routes to “ice I_c ” have been established, such as the dissociation of gas hydrates, warming amorphous ices or annealing high-pressure ices recovered at ambient pressure, freezing of μ - or nano-confined water (see ref. ¹). Despite the numerous studies on “ice I_c ”, its structure has not been fully verified, because the diffraction patterns of “ice I_c ” show signatures of stacking disorder^{1,8,9}, and ideal ice I_c without stacking disorder had not been formed until very recently¹⁰. This is the reason why “ice I_c ” is double-quoted¹, and it is recently proposed that the stacking-disordered ice should not be termed as ice I_c , but as ice I_{sd} ⁸.

“Ice I_c ” (ice I_{sd}) is known as a metastable form of ice at atmospheric pressure. But, recent computer simulations suggest that even ice I_{sd} could be the stable phase for crystallites up to sizes of at least 100,000 molecules¹¹. The stability of stacking-disordered ices is extremely important because of the ubiquitous nature of ice. Stacking-disordered ice can be characterized by the degree of ice cubicity, χ , which is defined as the fraction of cubic stacking^{1,8,9,12,13}. Until very recently, the highest cubicity was limited to ~80%^{8,14}, but it has been reported that ideal ice I_c with 100% cubicity has been obtained by annealing ice XVII¹⁰.

Recently new ice polymorphs, ice XVI¹⁵ and ice XVII^{16,17} are obtained by degassing gas molecules from neon and hydrogen hydrates, respectively. From these findings, we hypothesized that ideal ice I_c could be obtained by degassing hydrogen from hydrogen hydrate, C_2 . Five different phases in the H_2 – H_2O system have been reported to date (see ref. ¹⁸): Among them, neutron diffraction experiments have never been conducted for the higher-pressure phases, C_1 and C_2 , probably due to the technical difficulty in loading hydrogen into a pressure vessel, or compressing it to pressures in the giga-pascal range. To synthesize ideal ice I_c , decompression under low-temperature conditions for degassing is necessary, which is also not straight-forward using conventional pressure-temperature controlling systems. We have developed a Mito system¹⁹, and have overcome these technical difficulties (see details in Methods).

Here we present the neutron and X-ray diffraction results showing ice I_c without stacking disorder, obtained from degassing hydrogen hydrate C_2 . We also report an unexpected amorphous-like state in the transformation from C_2 to ice I_c , and the thermal stability of ice I_c .

Results

The route to obtain ice I_c . We started by using a mixture of D_2O and MgD_2 , which is an internal deuterium source, to synthesize hydrogen hydrate, C_2 . After loading the mixture into a pressure-temperature controlling system, MgD_2 was decomposed by heating at 403 K and at ca. 0 GPa for 1 h through a nominal reaction of $MgD_2 + 3D_2O \rightarrow Mg(OD)_2 + 2D_2 + D_2O$ (at b in Fig. 1, the observed neutron diffraction patterns are shown in Supplementary Fig. 1). Then, the samples were cooled to room temperature (at c in Fig. 1) and typically compressed up to ~3 GPa until a C_2 phase was observed (at d in Fig. 1).

The neutron diffraction pattern for the C_2 phase obtained at 3.3 GPa and 300 K (at d in Fig. 1) was analyzed by the Rietveld method. We adopted a splitting site model for guest D atoms located at the $48f$ site ($x, 1/8, 1/8$), and the host structure was identical to ice I_c ⁹ ($Fd\bar{3}m$, O at the $8b$ site ($3/8, 3/8, 3/8$), D at the

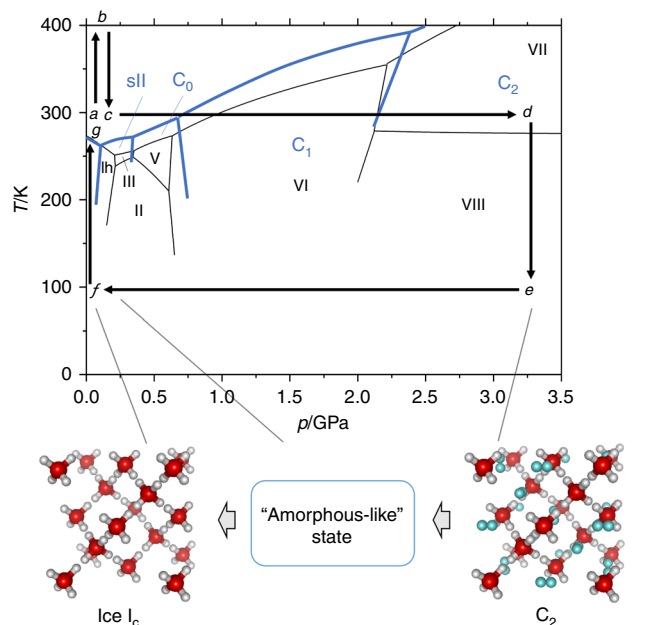


Fig. 1 Phase diagram of hydrogen hydrate and ice with experimental paths in this study. Phase boundaries for hydrogen hydrates and ices are drawn using thick blue lines and thin black lines, respectively. Experimental p - T paths are shown as black arrows in alphabetical sequence from a to g . The structural models for a high-pressure form of hydrogen hydrate, C_2 , and ice I_c are schematically drawn with a newly found amorphous-like state as an intermediate transitional state from C_2 to ice I_c . Red, white, and light blue balls in the structure model depict oxygen, hydrogen in water molecules, and hydrogen in guest molecules, respectively. Note that hydrogens in water molecules are disordered, so that two of four possible sites surrounding one oxygen are actually occupied.

$32e$ site (x, x, x)). The calculated diffraction pattern was in good agreement with the observed one, as shown in Fig. 2a. The refined structural parameters are listed in Supplementary Table 1.

The sample was then cooled from 300 K to 100 K at around 3 GPa (path $d \rightarrow e$). In the diffraction pattern taken at e in Fig. 1, peaks from solid deuterium (phase I) appeared at around 200 K (Supplementary Fig. 2), which is consistent with the known melting curve of hydrogen²⁰. This observation indicates that fluid deuterium coexisted with C_2 through the path from b to d .

The C_2 phase persisted at pressures at least as low as 0.5 GPa on decompression at 100 K (path $e \rightarrow f$). However, surprisingly, the Bragg peaks of C_2 mostly disappeared at 0.2 GPa (Fig. 3). This phenomenon is totally unexpected, because the host structure of gas hydrates retains its framework in the previous cases with ice XVI¹⁵ and XVII¹⁶. The sample was further decompressed to 0 GPa and evacuated using a turbo-molecular-pump. The broad peaks corresponding to ice I_c appeared at this stage. The peak disappearance of C_2 before the appearance of ice I_c was reproducibly observed in at least two separate neutron runs and one X-ray diffraction run for a hydrogenated sample (Supplementary Fig. 3). In the neutron diffraction pattern at 0.2 GPa, except for the Bragg peaks from $Mg(OD)_2$, only a broad peak was observed at around $d = 3.75$ Å, which was between the peak positions of 111 of C_2 and that of Ice I_c (Fig. 3). This fact implies that this state does not have long-range periodicity like a normal crystal, but has only local-ordering like an amorphous or nano-crystal. Considering the observed d -spacing, this amorphous-like form would be an intermediate transition state from C_2 to ice I_c , which forms while hydrogen molecules are partially degassed. It is highly likely that this apparent amorphization is derived from the

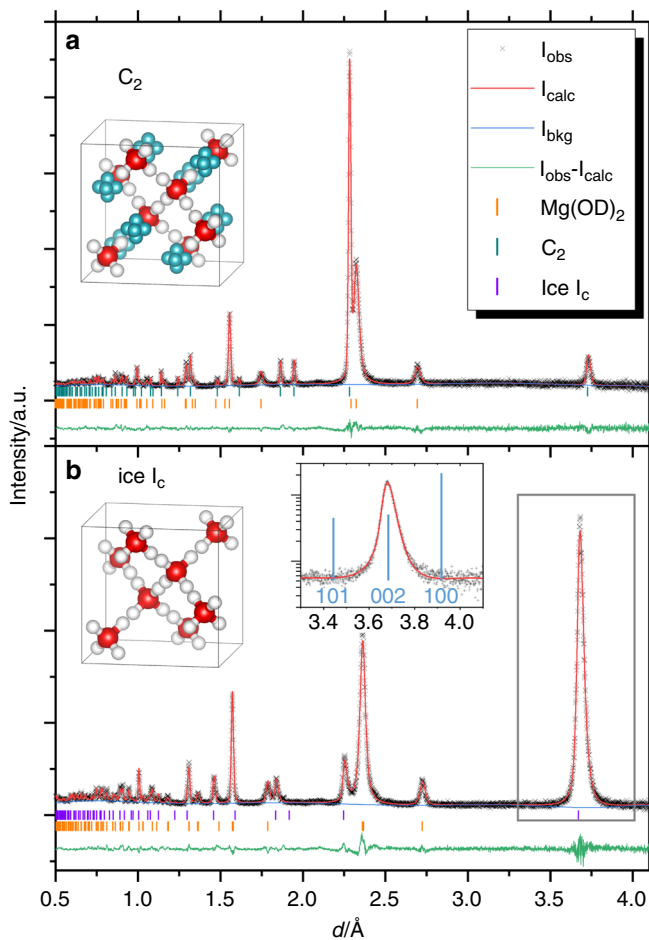


Fig. 2 Results of Rietveld analyses for neutron diffraction patterns. The patterns of **a** hydrogen hydrate, C_2 , and **b** ice I_c were obtained at 3.3 GPa and 300 K (at d in Fig. 1), and at 0 GPa and 130 K (in the path $f \rightarrow g$). The inset diffraction pattern in **b** shows the expanded area for 111 reflections, shown as a box in the main figure, with logarithmic scale. The calculated peak positions of ice I_h are also shown as light blue lines with their indices in the inset. Structure models for C_2 and ice I_c are also shown as insets in **a** and **b**, respectively.

lattice mismatch between C_2 and ice I_c , originating from the relatively small cage in the host framework of the ice I_c structure.

From the X-ray diffraction run, ice I_c , which may partially include molecular hydrogen, even appeared at 0.1 GPa through the transition from the C_2 phase to the amorphous-like state, even under pressure (Supplementary Fig. 3). This also represents a difference from the previous cases of ice XVI and XVII; ice XVI is formed under evacuation¹⁵, and hydrogen molecules can be refilled into ice XVII at an order of 10 bar of pressure¹⁶. It is worth noting that the partially degassed states are allowed in the cases of both ice XVI and XVII, so that the guest molecules can be continuously degassed from a fully occupied state to an empty state. The observed phase-separation behavior even under pressure in the ice H_2 - H_2O system indicates that the partially degassed C_2 phase would be unstable compared to the fully occupied or emptied phases, probably due to their lattice-mismatch.

The Bragg peaks in the neutron diffraction pattern for ice I_c obtained at 100 K were still broad, probably due to the small crystallite size and/or the remaining guest hydrogen molecules. The peaks of ice I_c sharpened with increasing temperature. This sharpening is dependent not only on temperature but also on time, which indicates that it is kinetic behavior.

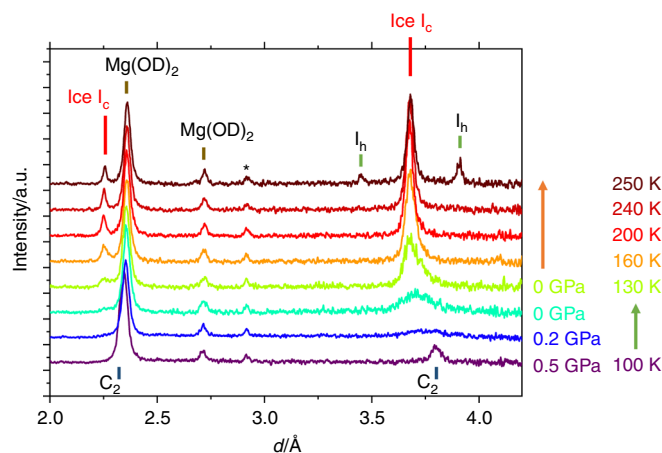


Fig. 3 Neutron diffraction patterns showing the transformation from C_2 to ice I_c . The patterns were obtained with decreasing pressure at 100 K (path $e \rightarrow f$) and with increasing temperature at 0 GPa (path $f \rightarrow g$). Corresponding temperatures and pressures are shown at the right side of the respective patterns, and the arrows mean that temperature or pressure kept constant. Most observed peaks are identified as C_2 , ice I_c , $Mg(OD)_2$, or ice I_h . The peak marked by an asterisk is a parasitic peak from the high-pressure cell.

Structure refinement for ice I_c . We conducted a separate run in order to obtain a neutron diffraction pattern for the structure refinement of the ice I_c . In this run, the neutron diffraction pattern was obtained at 130 K, which is well below the temperature at which the nucleation of ice I_h occurs²¹. We confirmed that the peak width did not change in the temperature region from 130 K to 180 K, such that the peak sharpening was almost complete, even at 130 K. The obtained neutron diffraction pattern was well fitted using the ice I_c structure model⁹, as shown in Fig. 2b and Supplementary Table 1. We also conducted the Rietveld analysis using C_2 structure model, and found that the occupancy of the D2 site is zero, within experimental error ($occ(D2) = -0.001(1)$). This shows that the guest hydrogen molecules are below the detectable limit at 130 K under evacuation. The peak profile around 111 peak of ice I_c has neither the feature of stacking disorder nor the peaks from ice I_h , as shown in the diffraction pattern in the region at around $d = 3.9$ Å, where the strongest 100 reflection of ice I_h is expected (see inset in Fig. 2b, and more detailed discussion for the peak broadening for ice I_c is described in Supplementary Note, Supplementary Table 2 and Supplementary Fig. 4). This should be a clear indication of the presence of ideal ice I_c without stacking disorder ($\chi = 100\%$)¹³, as clear as the recent discovery of ideal ice I_c by annealing ice XVII¹⁰.

Thermal stability of ice I_c . It is also noteworthy that the ice I_c surprisingly persists up to at least 240 K until ice I_h started to appear at 250 K (Fig. 3). The temperature of 240 K corresponds to the upper limit of the reported metastable region of “ice I_c ” (ice I_{sd})¹. However, in stacking-disordered ice, the cubic stacking sequence starts to change into a hexagonal stacking sequence at a much lower temperature, and the phase transition to ice I_h is completed at 240 K. The notable stability of the ice I_c would be derived from the lack of stacking disorder. The stacking-disordered ice has more dislocations, which promote the phase transformation from ice I_{sd} to ice I_h by reducing the activation energy required to change the stacking sequence²². This is also supported by a recent mesoscopic-size calculation²³. Note here that the critical temperature of 240 K has been identified as the temperature above which ice I_h without cubic stacking faults

forms spontaneously, which is the reason for the anomalous self-preservation regime of natural gas hydrates²⁴.

The diffraction pattern observed at 250 K looks a mixture of bulk ice I_c and I_h , rather than stacking-disordered ice with many stacking faults, judging from “stackogram” reported in the literatures^{8,13}. At 250 K, crystal growth would be dominant, rather than crystal nucleation. Therefore, once a crystallite nucleates, it quickly grows before other crystallites nucleate, resulting in the mixture of ice I_c and I_h , rather than stacking-disordered ice. This observation also suggests a smaller number of dislocations in the ice I_c observed in this study. On the contrary, the remarkable stability of the ice I_c and the bulk mixture of ice I_c and I_h at 250 K strongly support the conclusion that the obtained ice is not stacking-disordered, and it can therefore be called ice I_c without the need for quotation marks.

The discovery of ideal ice I_c will allow us to research the real physical properties of ice I_c without stacking disorder. For example, accurate heat capacity or vapor pressure measurements from low temperature will provide the free energy of ice I_c , which settle the long-standing argument for the thermodynamic stability of ice I_c compared to ice I_h . The physical properties of the ideal ice I_c are also important to understand how stacking disorder plays a role in the physical properties of ice I_{sd} . For instance, since the thermal conductivity of ice I_{sd} is significantly smaller than ice I_h ²⁵, the difference of thermal conductivities between ices I_h and I_c will emboss the effect of stacking disorder. It is also interesting what will be happened when ice I_c is compressed under low temperature; whichever ice I_c will be transformed into HDA (High Density Amorphous ice²⁶) or not? In any case, it is worth conducting what we previously did for ice I_h , to this ideal ice I_c as well.

Methods

Synthesis of MgD₂. MgD₂, used as the starting material in this study, was synthesized from reagent-grade MgH₂ as follows. MgH₂ powder (Wako pure chemical industries, Ltd.) was purchased and further ground in an agate mortar to increase the surface area, after which it was placed in a copper tube with a diameter of 4 mm and a length of 40 mm. The tube was mechanically sealed and but not welded, allowing the transfer of hydrogen gas. The copper tube was inserted into a 1/4” Inconel tube and connected in parallel to a deuterium gas cylinder and a turbo-molecular pump (TMP) with 1/16” stainless tubes and stop bulbs. The Inconel tube, including the sample copper tube, was heated to 773 K for 1 h using a tube furnace under evacuation using the TMP. Under these conditions, MgH₂ completely decomposed to Mg and H₂²⁷, and the degassed H₂ was evacuated. Then, the D₂ gas was introduced up to 4 MPa, and the temperature was cycled at the rate of 1 K/min between 673 K and 773 K while keeping the pressure at 4 MPa, which represents stable and unstable conditions for MgH₂²⁷, and this temperature cycle was repeated for 20 times. This activation process is necessary for the reaction $Mg + D_2 \rightarrow MgD_2$. Finally, the p - T conditions were maintained at 673 K and 4 MPa for 3 days to complete the reaction. The recovered sample was analyzed by powder X-ray diffraction (MiniFlex-II, Rigaku) and identified to be MgD₂ with a trace amount of MgO. Both MgD₂ and MgO react with D₂O and produce Mg(OD)₂, so this small amount of MgO does not affect the conclusion of this study.

Neutron diffraction and p - T control. Neutron powder diffraction experiments were conducted at the beamline PLANET²⁸ in the Material and Life Science Experiment Facility (MLF) of J-PARC, Ibaraki, Japan. The incident beam consists of 25 Hz pulsed spallation neutrons produced from a liquid Hg target via a decoupled moderator and traveled through collimators, choppers and supermirror guides to the sample positioned at 25.0 m from the moderator²⁸. Approx. 20 mg of MgD₂, synthesized as described above, was filled into TiZr null scattering gaskets, and D₂O water (99.9%, Wako pure chemical industries, Ltd.) was dropped on the MgD₂ powder, resulting in the molar ratio of MgD₂:D₂O~1:3. The gaskets were sandwiched between a pair of tungsten carbide anvils, and loaded by using a hybrid Mito system, which is a modified version of an original pressure-temperature variable Mito system¹⁹. The hybrid Mito system uses both flowing liquid nitrogen and a 4 K cryostat (RDK-415D, Sumitomo Heavy Industries, Ltd.), which allows us to control temperature rapidly, owing to the large latent heat of liquid nitrogen and efficient thermal insulation by zirconia and GFRP seats. The hybrid Mito system also allows us to achieve temperatures below 77 K, and reach a minimum temperature of ~35 K, owing to the cryostat. Another remarkable feature of the hybrid Mito system is that it affords pressure control, even at low temperature, as well as the original Mito system, which is indispensable for this study. Flexible copper

cloths were attached on the support rings of the anvils, and the cloths were placed in contact with the cold head of the cryostat for thermal conduction. The accessible minimum temperature of the hybrid Mito system is ~35 K, which may be the current technical limitation due to an unavoidable influx of heat from the surrounding cell. The sample pressure was estimated from the observed lattice parameter of Mg(OD)₂ brucite using the equation of states²⁹ and the observed unit cell volume of brucite at 0 GPa, assuming the temperature derivative of the bulk modulus of brucite, dK/dT , was ~0. Although this assumption may cause some error in the pressure estimated at low temperature, we placed emphasis on avoiding unwanted Bragg peaks from additional sources of pressure marker. Moreover, the error would be too small to affect the conclusion. The sample position was aligned by scanning to maximize the sample scattering intensity. The obtained intensities from the sample in the cell was subtracted by the intensity of the empty cell, and subsequently normalized by the attenuation corrected intensity of vanadium pellet in the cell, which was also subtracted by the intensity of the empty cell³⁰. The Rietveld analyses were performed using the GSAS³¹ with EXPGUI³², and the crystal structure was drawn with the VESTA program³³. The GSAS TOF profile function 3³¹ is used as the profile function in the Rietveld analyses.

X-ray diffraction. Powder X-ray diffraction measurements using a H₂O (Milli-Q) and MgH₂ (Wako pure chemical industries, Ltd.) mixture as starting materials were performed at the beamline BL-18C in the Photon Factory (KEK, Tsukuba, Japan). Samples were exposed to 0.6134 Å monochromatized synchrotron radiation, and the diffracted scattering was detected by an imaging plate (IP). The pressure was generated using CuBe alloy diamond-anvil cells and the temperature was controlled using a 4 K GM cryostat (MiniStat, Iwatani Co.) equipped with a temperature controller (Model 335, Lakeshore). Sample pressure was estimated from the difference in the R1 line wavelengths of rubies inside and outside the sample chamber³⁴. The temperature was monitored using a Si-diode sensor inserted in the cold head edge. We confirmed that the measured temperature was almost the same as that of the diamond anvils after temperature stabilization. The experimental p - T path was basically identical to the case of neutron diffraction, as shown in Fig. 1, while the achieved pressure at path d was 4.1 GPa.

One conically shaped Boehler-Almax type diamond-anvil³⁵ with a 0.6 mm culet was placed in the direction of the detector with an opening angle of $2\theta < 40^\circ$, whereas a conventional anvil with a 0.8 mm culet was positioned in the direction of the X-ray source. A CuBe plate with a hole of diameter 0.3 mm and an initial thickness of 0.2 mm was used as a gasket. This gasket was not subjected to pre-indentation. The load was applied by driving the piston by bellows using a He gas cylinder. The bellows allow us to control pressure at a few kbar more precisely than conventionally used membranes.

DFT calculations. Quantum Espresso³⁶ was used for the DFT calculations^{37,38}. We used Perdew-Burke-Ernzerhof (so-called PBE) type nonempirical exchange-correlation functions³⁹ for this study. The pseudopotentials were derived using projector augmented-wave approximation⁴⁰. The dispersion effects were taken into account using the exchange-hole dipole moment method (XDM), which calculates coefficients for polynomial of DFT-D dispersion energy⁴¹ from the exchange-hole dipole moment calculated from simulated electron wave function^{42,43}. XDM damping function parameters are taken from⁴⁴. The enthalpies of four possible configurations for the ordered form of ice I_c were calculated within a unit cell with a kinetic energy cutoff of 70 Ry and a Brillouin zone k mesh of $8 \times 8 \times 8$. The cell parameters and atomic coordinates were optimized using BFGS quasi-Newtonian methods at atmospheric pressure.

Data availability

The primary data that support the plots within this paper and other finding of this study are available from the corresponding author on reasonable request. The neutron crystallographic coordinates for structures reported in this study have been deposited at the Cambridge Crystallographic Data Centre (CCDC), under deposition numbers 1973757, 1973759. These data can be obtained free of charge from The Cambridge Crystallographic Data Centre via www.ccdc.cam.ac.uk/data_request/cif.

Received: 23 September 2019; Accepted: 3 January 2020;

Published online: 03 February 2020

References

- Kuhs, W. F., Sippel, C., Falenty, A. & Hansen, T. C. Extent and relevance of stacking disorder in “ice I_c ”. *Proc. Natl Acad. Sci. USA* **109**, 21259–21264 (2012).
- Murphy, D. M. Dehydration in cold clouds is enhanced by a transition from cubic to hexagonal ice. *Geophys. Res. Lett.* **30**, 2230 (2003).
- Riikonen, M. et al. Halo observations provide evidence of airborne cubic ice in the Earth’s atmosphere. *Appl. Opt.* **39**, 6080–6085 (2000).
- Whalley, E. Scheiner’s halo: evidence for ice I_c in the atmosphere. *Science* **211**, 389–390 (1981).

5. Gronkowski, P. The search for a cometary outbursts mechanism: a comparison of various theories. *Astronomische Nachrichten: Astronomical Notes* **328**, 126–136 (2007).
6. Prialnik, D. & Bar-Nun, A. Crystallization of amorphous ice as the cause of comet P/Halley's outburst at 14 AU. *Astron. Astrophys.* **258**, L9–L12 (1992).
7. König, H. Eine kubische Eismodifikation. *Z. Kristallogr. Cryst. Mater.* **105**, 279 (1943).
8. Malkin, T. L. et al. Stacking disorder in ice I. *Phys. Chem. Chem. Phys.* **17**, 60–76 (2015).
9. Kuhs, W. F., Bliss, D. V. & Finney, J. L. High-resolution neutron powder diffraction study of ice-Ic. *J. Phys.* **48**, 631–636 (1987).
10. del Rosso, L. et al. Cubic ice Ic free from stacking defects synthesized from ice XVII. Preprint at <https://arxiv.org/abs/1907.02915> (2019).
11. Lupi, L. et al. Role of stacking disorder in ice nucleation. *Nature* **551**, 218 (2017).
12. Malkin, T. L., Murray, B. J., Brukhno, A. V., Anwar, J. & Salzmann, C. G. Structure of ice crystallized from supercooled water. *Proc. Natl Acad. Sci. USA* **109**, 1041–1045 (2012).
13. Hansen, T. C., Sippel, C. & Kuhs, W. F. Approximations to the full description of stacking disorder in ice I for powder diffraction. *Z. für Kristallographie* **230**, 75–86 (2015).
14. Amaya, A. J. et al. How Cubic Can Ice Be? *J. Phys. Chem. Lett.* **8**, 3216–3222 (2017).
15. Falenty, A., Hansen, T. C. & Kuhs, W. F. Formation and properties of ice XVI obtained by emptying a type sII clathrate hydrate. *Nature* **516**, 231–233 (2014).
16. del Rosso, L., Celli, M. & Ulivi, L. New porous water ice metastable at atmospheric pressure obtained by emptying a hydrogen-filled ice. *Nat. Commun.* **7**, 13394 (2016).
17. del Rosso, L. et al. Refined structure of metastable ice XVII from neutron diffraction measurements. *J. Phys. Chem. C* **120**, 26955–26959 (2016).
18. Donnelly, M. E., Teerachanan, P., Bull, C. L., Hermann, A. & Loveday, J. S. Ostwald's rule of stages and metastable transitions in the hydrogen–water system at high pressure. *Phys. Chem. Chem. Phys.* **20**, 26853–26858 (2018).
19. Komatsu, K. et al. Development of a new P–T controlling system for neutron-scattering experiments. *High. Press. Res.* **33**, 208–213 (2013).
20. Diatschenko, V. et al. Melting curves of molecular hydrogen and molecular deuterium under high pressures between 20 and 373 K. *Phys. Rev. B* **32**, 381–389 (1985).
21. Hansen, T. C., Koza, M. M., Lindner, P. & Kuhs, W. F. Formation and annealing of cubic ice: II. Kinetic study. *J. Phys.: Condens. Matter* **20**, 285105 (2008).
22. Hondoh, T. Dislocation mechanism for transformation between cubic ice I_c and hexagonal ice I_h. *Philos. Mag.* **95**, 3590–3620 (2015).
23. Chan, H. et al. Machine learning coarse grained models for water. *Nat. Commun.* **10**, 379 (2019).
24. Kuhs, W. F., Genov, G., Staykova, D. K. & Hansen, T. Ice perfection and onset of anomalous preservation of gas hydrates. *Phys. Chem. Chem. Phys.* **6**, 4917–4920 (2004).
25. Johari, G. P. & Andersson, O. Effects of stacking disorder on thermal conductivity of cubic ice. *J. Chem. Phys.* **143**, 054505 (2015).
26. Mishima, O., Calvert, L. D. & Whalley, E. 'Melting ice' I at 77 K and 10 kbar: a new method of making amorphous solids. *Nature* **310**, 393–395 (1984).
27. Crivello, J.-C. et al. Review of magnesium hydride-based materials: development and optimisation. *Appl. Phys. A* **122**, 97 (2016).
28. Hattori, T. et al. Design and performance of high-pressure PLANET beamline at pulsed neutron source at J-PARC. *Nucl. Instr. Meth. Phys. Res. A* **780**, 55–67 (2015).
29. Horita, J., dos Santos, A. M., Tulk, C. A., Chakoumakos, B. C. & Polyakov, V. B. High-pressure neutron diffraction study on H–D isotope effects in brucite. *Phys. Chem. Miner.* **37**, 741–749 (2010).
30. Komatsu, K. et al. Crystal structure of magnesium dichloride decahydrate determined by X-ray and neutron diffraction under high pressure. *Acta Crystallogr. B* **71**, 74–80 (2015).
31. Larson, A. & Von Dreele, R. General Structure Analysis System (GSAS). Los Alamos National Laboratory, Report LAUR-86-748 (2004).
32. Toby, B. EXPGUI, a graphical user interface for GSAS. *J. Appl. Crystallogr.* **34**, 210–213 (2001).
33. Momma, K. & Izumi, F. VESTA 3 for three-dimensional visualization of crystal, volumetric and morphology data. *J. Appl. Crystallogr.* **44**, 1272–1276 (2011).
34. Piermarini, G. J., Block, S., Barnett, J. D. & Forman, R. A. Calibration of the pressure dependence of the R₁ ruby fluorescence line to 195 kbar. *J. Appl. Phys.* **46**, 2774–2780 (1975).
35. Boehler, R. & De Hantsetters, K. New anvil designs in diamond-cells. *High. Press. Res.* **24**, 391–396 (2004).
36. Paolo, G. et al. QUANTUM ESPRESSO: a modular and open-source software project for quantum simulations of materials. *J. Phys. Condens. Matter* **21**, 395502 (2009).
37. Hohenberg, P. & Kohn, W. Inhomogeneous electron gas. *Phys. Rev.* **136**, B864–B871 (1964).
38. Kohn, W. & Sham, L. J. Self-consistent equations including exchange and correlation effects. *Phys. Rev.* **140**, A1133–A1138 (1965).
39. Perdew, J. P., Burke, K. & Ernzerhof, M. Generalized gradient approximation made simple. *Phys. Rev. Lett.* **77**, 3865–3868 (1996).
40. Kresse, G. & Joubert, D. From ultrasoft pseudopotentials to the projector augmented-wave method. *Phys. Rev. B* **59**, 1758–1775 (1999).
41. Grimme, S., Antony, J., Ehrlich, S. & Krieg, H. A consistent and accurate ab initio parametrization of density functional dispersion correction (DFT-D) for the 94 elements H–Pu. *J. Chem. Phys.* **132**, 154104 (2010).
42. Becke, A. D. & Johnson, E. R. Exchange-hole dipole moment and the dispersion interaction. *J. Chem. Phys.* **122**, 154104 (2005).
43. Becke, A. D. & Johnson, E. R. Exchange-hole dipole moment and the dispersion interaction revisited. *J. Chem. Phys.* **127**, 154108 (2007).
44. Otero-de-la-Roza, A. & Johnson, E. R. Van der Waals interactions in solids using the exchange-hole dipole moment model. *J. Chem. Phys.* **136**, 174109 (2012).

Acknowledgements

We are grateful to Drs. J. Abe and K. Funakoshi for their assistance with the experiments, and to anonymous reviewers for their valuable comments, particularly on the relation with anomalous preservation of gas hydrates. Neutron diffraction experiments were performed through the J-PARC user programs (Nos. 2014B0187, 2015A0033, 2017A0092, 2017B0031). X-ray diffraction experiments were performed under the approval of the Photon Factory Program Advisory Committee (Proposal Nos. 2016G107, 2018G656). This study was supported by JSPS KAKENHI (Grant Numbers: 18H05224, 18H01936, 15H05829).

Author contributions

K.K. and S.M. conceived and designed the experiments. K.K., S.M., T.H., A.S-F., R.Y., K.Y., and H.K. conducted the neutron diffraction experiments. K.K., R.Y., K.Y., and H.K. conducted the X-ray diffraction experiments. F.N. carried out the DFT calculations and wrote the corresponding part of the manuscript. K.K. analyzed the data and wrote the manuscript with contributions from all authors.

Competing interests

The authors declare no competing interests.

Additional information

Supplementary information is available for this paper at <https://doi.org/10.1038/s41467-020-14346-5>.

Correspondence and requests for materials should be addressed to K.K.

Peer review information *Nature Communications* thanks John Loveday and the anonymous reviewer(s) for their contribution to the peer review of this work.

Reprints and permission information is available at <http://www.nature.com/reprints>

Publisher's note Springer Nature remains neutral with regard to jurisdictional claims in published maps and institutional affiliations.



Open Access This article is licensed under a Creative Commons Attribution 4.0 International License, which permits use, sharing, adaptation, distribution and reproduction in any medium or format, as long as you give appropriate credit to the original author(s) and the source, provide a link to the Creative Commons license, and indicate if changes were made. The images or other third party material in this article are included in the article's Creative Commons license, unless indicated otherwise in a credit line to the material. If material is not included in the article's Creative Commons license and your intended use is not permitted by statutory regulation or exceeds the permitted use, you will need to obtain permission directly from the copyright holder. To view a copy of this license, visit <http://creativecommons.org/licenses/by/4.0/>.

© The Author(s) 2020